arXiv:1210.6745v2 [astro-ph.EP] 26 Oct 2012

Fomalhaut b: Independent Analysis of the Hubble Space Telescope Public Archive Data

Raphaël Galicher[1,2], Christian Marois[1], B. Zuckerman[3], Bruce Macintosh[4]

[1]*National Research Council Canada, Dominion Astrophysical Observatory, 5071 West Saanich Road, Victoria, BC, V9E 2E7, Canada;*

[2]*Dept. de Physique, Université de Montréal, C.P. 6128 Succ. Centre-ville, Montréal, Qc, H3C 3J7, Canada;*

[3]*Department of Physics and Astronomy, University of California, Los Angeles, CA 90095, USA;*

[4]*Lawrence Livermore National Laboratory, 7000 East Ave., Livermore, California, 94550, USA;*

`raphael.galicher@obspm.fr`

Submitted to ApJ on Aug, 9th 2012

ABSTRACT

The nature and even the existence of a putative planet-mass companion ("Fomalhaut b") to Fomalhaut has been debated since 2008. In the present paper we reanalyze the multi-epoch Hubble Space Telescope (HST) optical images on which the discovery claim was based. We confirm that the HST images do reveal an object in orbit around Fomalhaut but the detailed results from our analysis differ in some ways from previous discussions. In particular, we do not confirm flux variability over a two-year interval at $0.6\,\mu$m wavelength, we detect Fomalhaut b for the first time at the short wavelength of $0.43\,\mu$m, we find that the HST image of Fomalhaut b at $0.8\,\mu$m may be extended beyond the PSF, and we cannot determine from our astrometry if Fomalhaut b will cross or not the dust ring. The optical through mid-infrared spectral energy distribution (SED) of Fomalhaut b cannot be explained as due to direct or scattered radiation from a massive planet. We consider two models to explain the SED: (1) a large circumplanetary disk around a massive, but unseen, planet and (2) the aftermath of a collision during the past 100 years of two Kuiper Belt-like objects of radii $\sim 50\,$km.

Subject headings: **Methods: data analysis, Methods: observational, Techniques: high angular resolution, Techniques: image processing, : planetary systems.**

1. Introduction

Direct imaging is the appropriate technique for the study of exoplanets with semi-major axis larger than a few astronomical units (Marois et al. 2008, 2010; Kalas et al. 2008; Lagrange et al. 2009). As the planetary atmospheric thermal emission or scattered light is detected, detailed multi-band photometry or spectrometry can be used to probe the atmospheric composition and physical properties. However, these studies are challenging given the very high contrast and small angular separation between a star and planet. In some systems the presence of a planet before it is detected directly can be suggested by the geometry of a circumstellar debris disk. For example, Wyatt et al. (1999), Kalas et al. (2005) and Quillen et al. (2006) had predicted the likely existence of a planet around Fomalhaut and Mouillet et al. (1997) of a planet around β-Pictoris.

In the case of Fomalhaut (440 ± 40 Myr, 7.7 pc, Mamajek 2012; Van Leeuwen 2007), a candidate planet was announced by Kalas et al. (2008, hereafter K08). Surprisingly, the candidate was not detected in deep near infrared images in H and Lp bands, but rather in Hubble Space Telescope (HST) images in the visible where planets are not expected to emit much thermal light. The K08 planet model that best fit the 2008 photometry is a $< 3M_\mathrm{J}$ Jovian planet surrounded by a large circumplanetary disk; the observed optical light is mostly scattered by the disk, not by the planet itself. In this model, it is assumed that Hα emission (dust accretion or hot planetary chromosphere) explains the unusual 50% variability of the reported flux at 0.6 μm over a two year time interval. Based on their astrometric mesurements, Kalas et al. (2010) also announced that Fomalhaut b is likely to cross the dust ring.

A few years later, as they could not detect the object at 4.5 μm with Spitzer, Janson et al. (2012) concluded that "there is almost certainly no direct flux from a planet contributing to the visible-light signature" and they proposed an optically thin dust cloud with or without a central object in the super-Earth regime to explain the K08 photometry. Kennedy&Wyatt (2011) also rejected direct detection of massive planets and explain the photometry at 0.6-0.8 μm to be a consequence of a swarm of satellites around a 2-100 M_Earth planet.

Motivated by the controversial status of Fomalhaut b within the community, including even doubts of its actual existence, we decided to conduct an independent analysis of the HST public data that were recorded in 2004, 2006 and 2010. After describing the observational method in § 2 and our data reduction in § 3, we analyze the images to confirm that Fomalhaut b is a convincingly real detection and that it is gravitationally bound to the star. In § 4.2 we study various possible orbits to determine if the current astrometry can confirm or reject a dust belt crossing trajectory (such as one announced by Kalas et al. 2010). In § 4 we estimate the object's photometry and possible origin as a circumplanetary disk around a planet or the aftermath of a collision of two Kuiper Belt-like objects, while considering that Fomalhaut b is not (§ 4.3) or is (§ 4.4) spatially resolved in the HST images.

Date (UT)	Instrument	Spot diam. (arcsec)	Filter	Im.	Exp. (sec)	Roll	FOV rot. (deg)
2004 Oct. 25-26	ACS/HRC	1.8	F606W	112	5615	3	8.0
2006 Jul. 14	ACS/HRC	1.8	F435W	9	6525	3	5.8
2006 Jul. 15-16	ACS/HRC	3.0	F435W	9	6435	3	5.8
2006 Jul. 19-20	ACS/HRC	3.0	F606W	28	7240	4	6.0
2006 Jul. 18	ACS/HRC	1.8	F814W	20	5280	3	6.0
2006 Jul. 19	ACS/HRC	3.0	F814W	27	4942	3	6.0
2010 Jun. 14	STIS/50CORON	2.5	CLEAR	3	630	7	157.0
2010 Sep. 13	STIS/50CORON	2.5	CLEAR	16	3000		

Table 1: *Fomalhaut observing log. Column ”Im.” gives the number of useful images. Column ”Exp.” is the total integrated time of the useful images. ”Roll” is the number of roll angles in the sequence and ”FOV rot.” gives the total FOV rotation during the sequence.*

2. Observations

The data that we consider in this paper were obtained with HST with the Advanced Camera for Surveys (ACS) in 2004 and 2006 (programs 10390 and 10598), and the Space Telescope Imaging Spectrograph instrument (STIS) in 2010 (program 11818). The ACS data were acquired with the High Resolution Channel (HRC) in its coronagraphic mode with 1.8” and 3.0” focal plane occulting masks and the F435W (430 ± 50 nm), F606W (595 ± 115 nm), and F814W (825 ± 115 nm) filters. For the STIS data, the 50CORON configuration was used with its clear aperture (600 ± 220 nm). For all sequences, images at several roll angles were taken so that the stellar diffraction pattern can be subtracted while keeping the flux of any point sources. Tab. 1 gives the dates of the observations, the instrument configurations (filter, coronagraph), the number of useful images with the corresponding integration time, and the number of roll angles as well as the total rotation of the field of view.

3. Data reduction

3.1. ACS

We start from the `drz` drizzled images produced by the ACS pipeline (geometric distortion, photometry, and cosmic ray calibrations). For each image, we create a map of pixels that deviate by more than $3.5\,\sigma$ in a 20×20 pixel box and we replace them with the median value in the box. We multiply each image by the PHOTFLAM of its header to convert the pixel counts to erg s^{-1} cm^{-2} Å^{-1} arcsec^{-2}. For the Fomalhaut PSF registration, we first start with the 2006 sequence at F606W that is recorded with the 3.0” focal plane mask. We align every image maximizing its correlation with the first image of the sequence (Table 1). The correlation is maximized in the annulus with inner and outer radii of 140 and 200 pixels where the central vertical band of width 240 pixel is removed (saturated detector) and where the coro-

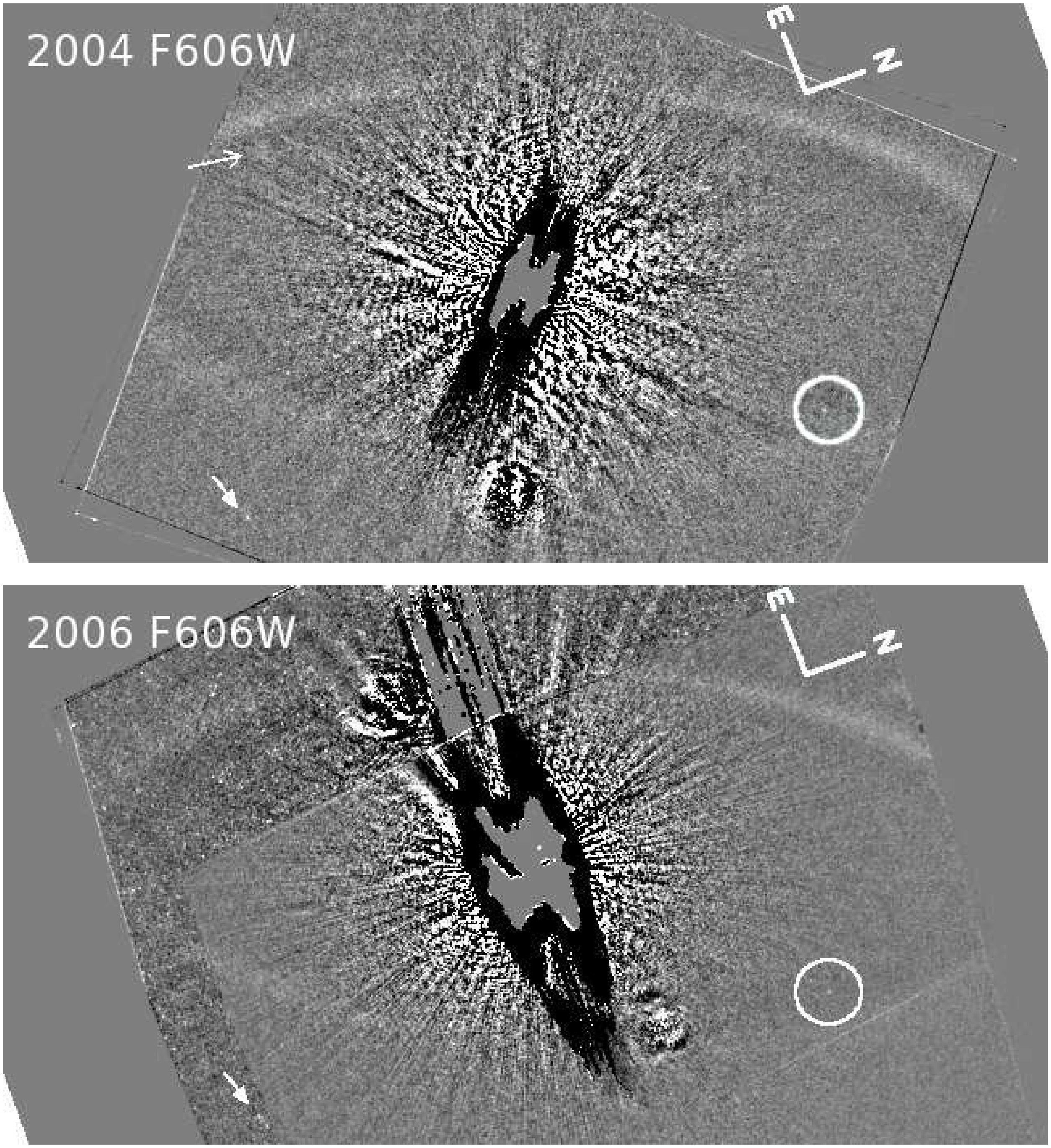

Fig. 1.— *ACS images of the dust belt and the object b (circle) around Fomalhaut at F606W in 2004 (top) and 2006 (bottom). Two arrows point to background sources. The length of the segments giving the East and North orientations is 2.5". The intensity scale is linear and it is the same for the two images.*

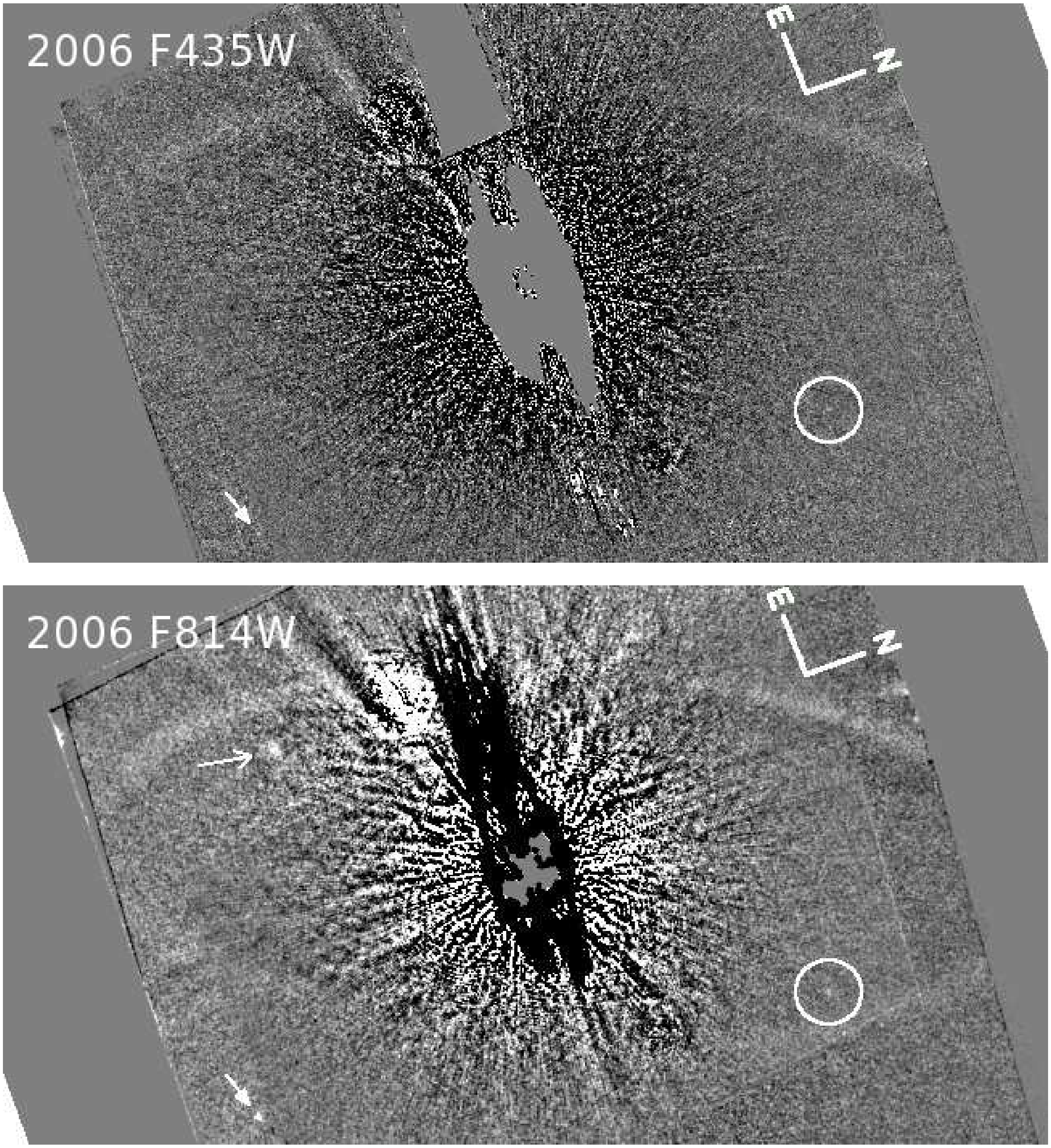

Fig. 2.— *Same as Fig. 1 for F435W (top) and F814W (bottom) ACS images taken in 2006.*

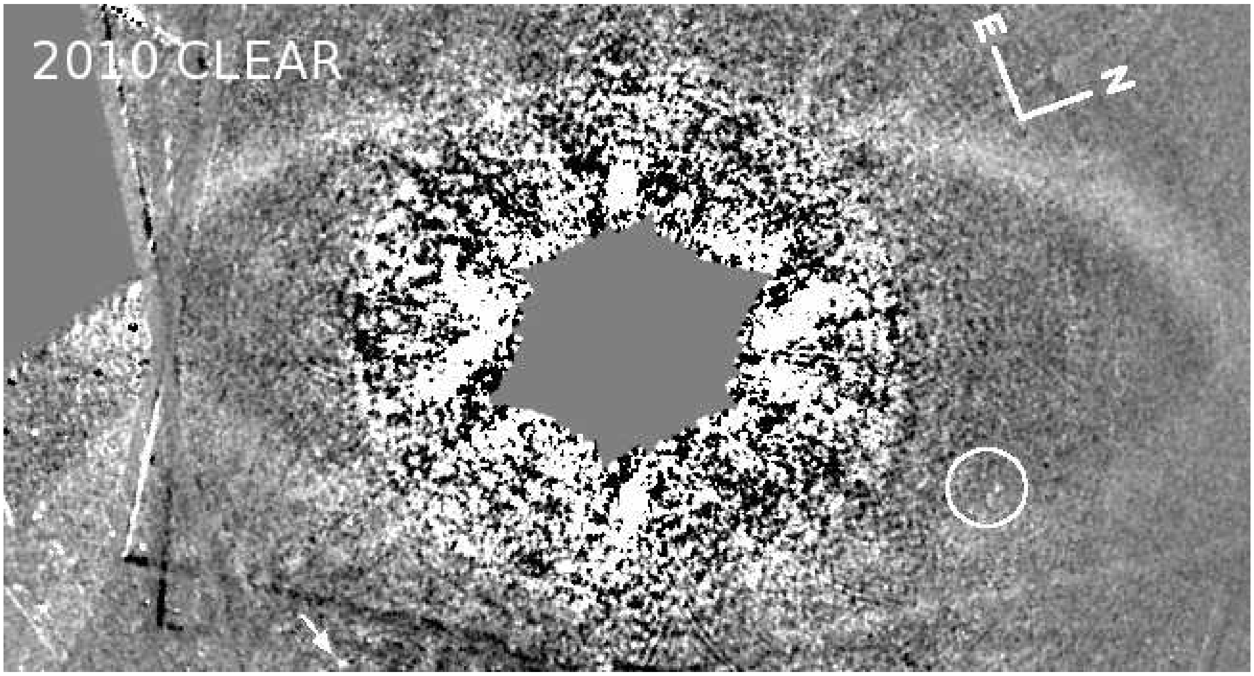

Fig. 3.— *Same as Fig. 1 for the STIS image taken in 2010 with the CLEAR filter.*

nagraphic focal plane bar is masked. We call this optimization area A. Once the images are aligned to within 0.1 pixel, the absolute center of the star PSF is found by median-combining the aligned images and by registering the resulting image to the image center by maximizing in A the cross-correlation of the diffraction spikes with themselves in a 180° rotation of the image about its center. This procedure defines the absolute center within 0.5 pixel and we call R606 the registered median-image. We then register all images of F606W sequences maximizing their cross-correlation with R606 in A. For the F435W and F814W sequences, we scale R606 to the corresponding wavelengths (814nm for F814W and 480nm[1] for F435W) and call R435 and R814 the resulting images. We then register all F435W and F814W images maximizing the cross-correlation in A with R435 and R814 respectively. For every sequence listed in Tab. 1, we then subtract the stellar speckles. As the field of view rotates only by a few degrees, there is almost no difference between applying a locally optimized combination of images algorithm (Lafrenière et al. 2007; Marois et al. 2010b) or a basic angular differential imaging data reduction as described in Marois et al. (2006). We choose the second procedure which is less time consuming. Considering one of the sequences, we subtract from each image a reference PSF that is the median of all images that were recorded at a different roll angle. We then rotate the images to put North up and median combine them. For the 2006 data, we work out the weighted mean of the reduced images taken with the 1.8" and 3.0" masks in the same filter. As the fields-of-view do not exactly overlap, the contrast is not the same in all parts of the images (Figs. 1 and 2). A point source (arrow) is detected in all images South West from Fomalhaut A. An extended object (red arrow, South East) is also detected in 2004 and in 2006 (F814W). The motion of these two sources between 2004 and 2006 are consistent with them being background objects. Fomalhaut b (inside the circles) is detected at F435W, F606W, and F814W with a signal-to-noise ratio of ∼ 3, 5-6, and 3 respectively and it does not have the same motion as the background sources (Fig. 4). We thus confirm that it is a real object orbiting Fomalhaut.

---

[1] Better match of the diffraction spikes than for 435nm.

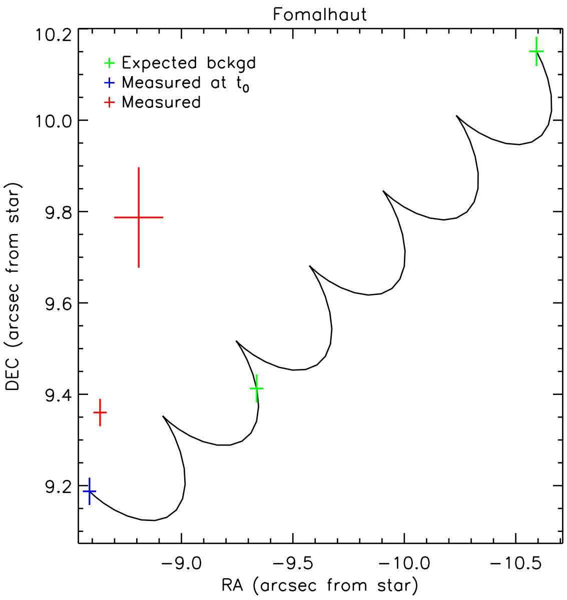

Fig. 4.— *Fomalhaut b measured positions in 2004, 2006 and 2010 images (red crosses) and expected positions for a background source (green crosses).*

3.2. STIS

The `sx2` images that are provided by the STIS pipeline (geometric distortions, photometry, and cosmic ray calibrations) are used for our analysis. The flux density is converted to erg s^{-1} cm^{-2} $Å^{-1}$ $arcsec^{-2}$ by multiplying each image by the PHOTFLAM of its header and dividing it by the exposure time. The spider spikes are well detected in these images and we register the first image of the sequence maximizing the cross-correlation of the spikes with themselves in a 180° rotation of the image about its center. The maximization was done around the spikes (±2 pixels) between 100 and 230 pixels from the star. We then register the other images maximizing the cross-correlation with the first image in the 200 pixel-radius disk where the 160 pixel central vertical band and the 30 pixel central horizontal band are masked. As the roll angles are well spread in the 0-157° interval, we apply a locally optimized combination of images algorithm (Lafrenière et al. 2007; Marois et al. 2010b) to suppress the stellar diffraction pattern. Using a LOCI algorithm, a PSF reference image is built for each image of the sequence and it is subtracted. After subtraction, the images are rotated to put North up and they are median-combined. The final image with the detection of Fomalhaut b is shown in Fig. 3.

4. Data analysis

4.1. Belt geometry

The geometrical properties of the belt have been discussed previously (Kalas et al. 2005; Acke et al. 2012; Boley et al. 2012) and it is beyond the scope of the present paper to refine them. However, we find an eccentric belt that reproduces the images, with an eccentricity e=0.10-0.11, a radius between 136-148 AU, a right ascension of ascending node 156.5-157°, an argument of periapsis 35°, and an inclination of 67°. All the parameters are in good agreement with the published values of K08 (31±6° for the argument of periapsis unlike the 1±6° found by Acke et al. (2012)). We did not use a mathematical fit to optimize values of parameters and our best visual fit is only used to estimate the belt geometry in our images.

4.2. Astrometry

We use the Tiny Tim (Krist et al. 2011) tool that generates HST template PSFs to build a model of a point source in our images at the position of Fomalhaut b to accurately estimate its astrometry and photometry. The temperature of a thermally emitting companion that would reproduce the F814W flux is roughly 400 K (Janson et al. 2012, hereafter J12). Thus, we choose a 400 K source in the Tiny Tim tool and we simulate the images prior to the speckle suppression to account for the ADI/LOCI effects, the rotation we apply to put north up, and the weights of the weighted means for the 2006 data. We then adjust the position and flux of the template to subtract from the image to minimize the residual noise in a 0.7" (1.2")-diameter disk centered on Fomalhaut b for the ACS (SITS) data. The positions we derive from the fit are given in Tab. 2. K08 measured in their images that Fomalhaut b is at [RA, DEC] = [-8.62", 9.20"] and [-8.60", 9.38"] from Fomalhaut A in 2004 and 2006 respectively. We estimate the difference δ_i between K08 positions and ours at epoch i as

$$\delta_i = \sqrt{\frac{\delta_i \mathrm{ra}^2 + \delta_i \mathrm{dec}^2}{\sigma_{\mathrm{ra,i}}^2 + \sigma_{\mathrm{dec,i}}^2}} \tag{1}$$

where $\delta_i$ra and $\delta_i$dec are the difference between K08 measurements and ours of the offset along the West-East direction and the South-North direction respectively. $\sigma_{\mathrm{ra,i}}$ and $\sigma_{\mathrm{dec,i}}$ are our error bars (K08 give no error bars). We find that our positions are within $1.5\,\sigma$ of K08 positions at the two epochs 2004 and 2006 (i.e. $\delta_i \lesssim 1.5$). The difference with K08 could result from a different registering technique or from differences in the ACS pipeline that have been upgraded since 2008.

As we have only three epochs close in time and large error bars for the 2010 data, we cannot strongly constrain the orbital parameters. We then consider only two keplerian orbits – one that crosses the dust ring and a second that does not cross the ring – and compare the expected and measured positions.

The first orbit is a 0.19 eccentric orbit with a 118 AU semi-major axis, a 156° right ascension of the ascending node, a 70° inclination, and a 2° argument of periapsis. The orbit does not cross the dust ring and is represented in dashed lines in Fig. 5 where the dust belt is bound by dashed-dotted lines. We use Eq. 1 replacing K08 positions with the expected positions of Fomalhaut b on the keplerian orbit to estimate the differences δ_i between the expected positions and our measurements at each epoch i (2004, 2006, and 2010). Then, we estimate the total difference as $\delta = \sum_i \delta_i$. We find that the expected positions are $1.1\,\sigma$ from the measured posi-

Date	Filter	Offset from A to b		Separation	PA
		RA (")	DEC (")	(")	(deg)
2004 Oct. 25-26	F606W	-8.59±0.02	9.19±0.02	12.58±0.03	316.9±0.1
2006 Jul. 14-15-16	F435W	-8.61±0.03	9.36±0.03	12.72±0.04	317.4±0.2
2006 Jul. 19-20	F606W	-8.64±0.02	9.36±0.02	12.73±0.03	317.3±0.1
2006 Jul. 18-19	F814W	-8.64±0.03	9.36±0.03	12.73±0.04	317.3±0.2
2010 Jun. 14-Sep. 13	CLEAR	-8.81±0.07	9.79±0.07	13.17±0.10	318.0±0.4

Table 2: *Fomalhaut b astrometry with respect to Fomalhaut A.*

tions ($\delta = 1.1$). The second keplerian orbit (full lines) we consider has an eccentricity 0.25, a semi-major axis 119 AU, a right ascension of the ascending node 156°, an inclination 70°, and an argument of periapsis 10°. The difference between expected and measured positions is $0.9\,\sigma$. If Fomalhaut b follows this orbit, it will enter the dust belt in ~ 100 years. Given these two examples, new data are obviously required to conclude whether Fomalhaut b will or will not cross the belt.

4.3. Fomalhaut b as a point source

We consider Fomalhaut b as a point source in this section. We estimate its photometry and compare our results with K08 fluxes (§ 4.3.1). We then examine models discussed by K08 and J12 (§ 4.3.2 and § 4.3.3).

4.3.1. Photometry

For each filter and epoch, we derive the photometry by integrating the flux density of the PSF template that best fits the data (§ 4.2) in a 1.25" radius disk for the ACS data and 1" radius for the STIS data. The fractions of the PSF integrated energy inside these apertures are 0.960, 0.961, 0.918, and 0.996 for the F435W, F606W, F814W, and CLEAR/STIS filters respectively. To convert the estimated flux densities F_λ in erg s^{-1} cm^{-2} Å^{-1} to flux densities F_ν in erg s^{-1} cm^{-2} Hz^{-1} (i.e. 10^{23} Jy), we use the PHOTPLAM keyword recorded by the ACS and STIS pipelines in the fits headers:

$$F_\nu = F_\lambda \text{ photplam}^2\ 10^{-18.4768} \quad (2)$$

The resulting flux densities (μJy) are given in Tab. 3. The error bars σ_ν in percentage are the inverse of the signal-to-noise ratios. In these ratios, the signal is the integrated flux density inside a 0.2" radius disk centered on Fomalhaut b and the noise is the square root of the total variance of the residual noise after subtraction of the best PSF in the same area. K08 express

Date	Filter	Flux density (μJy)	
			Kalas
2004	F606W	0.69±0.11	0.61±0.05
2006	F435W	0.41±0.15	<0.87 ($5\,\sigma$)
2006	F606W	0.47±0.09	0.29±0.03
2006	F814W	0.38±0.12	0.37±0.04
2010	CLEAR	0.88±0.32	

Table 3: *Photometry if Fomalhaut b is a point source.*

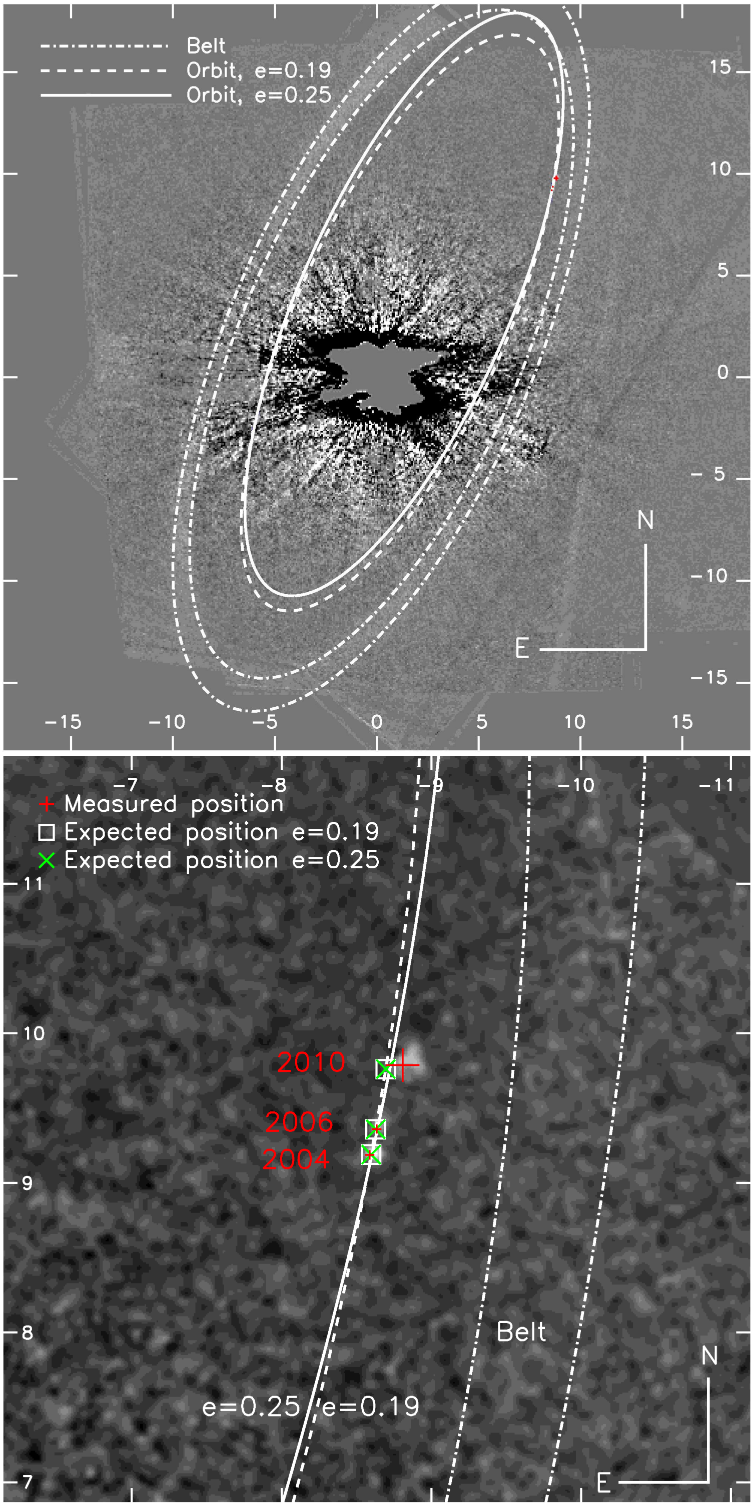

Fig. 5.— *Trajectories that best fits the Fomalhaut b positions with eccentricity 0.19 (dashed lines) or 0.25 (full line).*

their Fomalhaut b photometry and upper limits in Vega magnitudes. We convert their measurements to μJy (last column in Tab. 3) using the ACS handbook.

Most of the flux densities (Tab. 3) are consistent with K08 values except our F606W/2006 point which is $\sim 2\,\sigma$ brighter (σ is the quadratic sum of K08 error bars and ours). Moreover, our error bars are larger than K08's ones. Thus, even if we still detect a variability in the F606W filter between 2004 and 2006, it is not as significant ($1.5\,\sigma_G$) as it is in K08 (5-$6\,\sigma_K$) – where σ_G and σ_K are our error bars and K08 ones respectively. We also find that the flux density measured in the CLEAR filter (its bandpass roughly corresponds to F435W+F606W+F814W) is consistent with the three ACS flux densities given the large error bar. Finally, we (marginally) detect Fomalhaut b at F435W unlike K08 who have an upper limit.

We plot the photometry of our detections (crosses) in Fig. 6 along with upper limits from the literature (K08, Marengo et al. 2009, and J12) at various wavelengths. J12 find that to comply with their $4.5\,\mu$m upper limit, the planetary mass upper limit is $1 M_J$ at 400 Myr. Thus, we compare the measurements with a model of a cloud-free atmosphere for a $1\,M_J$ planet at 400 Myr with the solar metallicity (Siegel&Burrows 2012) (full line in Fig. 6). It is clear that a planet-only model for Fomalhaut b is not consistent with the observations. K08 proposed two other models: a cloud of dust (§ 4.3.2) or a disk of dust around a Jovian-planet (§ 4.3.3). We revisit these two models in light of our updated photometry.

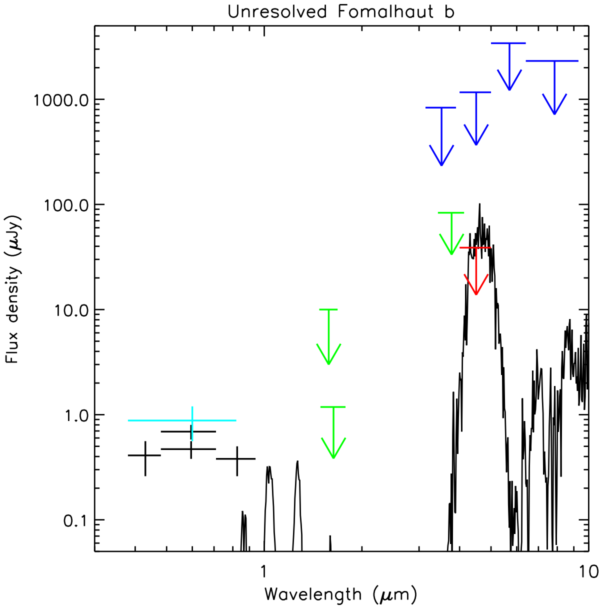

Fig. 6.— *Fomalhaut b flux density (μJy) for various wavelengths (μm^{-1}) in the case the object is unresolved. Crosses correspond to our detections (four black for ACS and one light blue for STIS). Arrows are upper limits from the literature: green, red, and blue for K08, J12, and Marengo et al. (2009) respectively. The solid line represent a cloud-free atmosphere model for a $1\,M_J$ planet at 400 Myr.*

4.3.2. Cloud of dust

We consider the model introduced in K08 with a 0.53 AU diameter cloud composed of dust grains with a differential size distribution $dn/da \propto (a/a_0)^{-3.5}$ where the radius a goes from $a_{\rm min}$ to $1000\,\mu$m. Using Mie theory, K08 calculate the apparent magnitudes of such a cloud composed of water ice (density=1, $m_{\rm ice}$) or refractory carbonaceous material (density=2.2, $m_{\rm LG}$) with $a_{\rm min} = 0.01\,\mu$m (hereafter $m^{0.01}$) or $8\,\mu$m (hereafter m^8). The total mass in grains is adjusted such that the integrated light in F814W from the model matches K08's observations (K08's and our photometry in F814W are in agreement). We convert the Vega magnitudes provided in K08's Tab. S3 to flux densities in μJy (Tab. 4). The last line gives the error ϵ between the expected flux densities $F_{e,\nu}$ and the observed densities F_ν:

$$\epsilon = \sqrt{\sum_\nu \frac{(F_\nu - F_{e,\nu})^2}{\sigma_\nu^2}} \tag{3}$$

Filter	$m_{\rm ice}^{0.01}$	$m_{\rm LG}^{0.01}$	$m_{\rm ice}^{8}$	$m_{\rm LG}^{8}$
F435W	0.71	0.58	0.63	0.46
F606W	0.55	0.50	0.46	0.45
F814W	0.37	0.37	0.37	0.37
ϵ	2.0	1.3	1.7	1.0

Table 4: *Expected flux densities $F_{e,\nu}$ (μJy) derived from the cloud models ($m_{\rm ice}^{0.01}$, $m_{\rm LG}^{0.01}$, $m_{\rm ice}^{8}$, and $m_{\rm LG}^{8}$) proposed in K08. The last line gives the difference between $F_{e,\nu}$ and our measured photometry F_ν (see text for details).*

K08 reject the possibility that Fomalhaut b can be explained by one of these cloud models because 1/ they do not detect the object at F435W (they do not reject $m_{\rm LG}^{8}$ for this reason), 2/ the red color they observe does not match the model, and 3/ they cannot explain the F606W variability. All these reasons do not apply to our new photometry because 1/ we detect Fomalhaut b at F435W, 2/ the expected flux densities match the observed flux densities within 1.7 σ for three of the four models ($\epsilon < 1.7$), and 3/ the F606W variability is not significant in our images. K08 also explain that such a cloud could result from a collision of two planetesimals and that the probability of such an event is lower at the Fomalhaut b position than closer to the star or closer to the belt. However, as suggested by J12, the probability of a collision is not the probability of its detection because the speckle noise and the high brightness of the ring may prevent detections of such clouds close to the star and the belt respectively. Finally, K08 argue that such dust clouds would be sheared due to differential gravitational forces and rapidly spatially resolved by HST. However, assuming a cloud with diameter 0.5 AU only subject to gravitational forces from the star, we find that its image would be larger than 2 pixels (~FWHM) and 4 pixels after ~100 years and ~200 years respectively. It would take ~500 years to shear the cloud of dust so that it could be spatially resolved in the HST images with no doubt. Thus, we find no strong arguments to reject K08 models of a dust cloud with radius ~ 0.5 AU, composed of water ice or refractory carbonaceous small grains, and younger than ~ 500 years.

4.3.3. Material surrounding a Jupiter-like planet

A second scenario proposed by K08 is an unseen Jovian planet surrounded by a disk of dust with a radius of 16-35 planet radius. As the K08 photometry is close to ours and K08 only work out rough numbers (they could not constrain all the parameters with only two photometric points), the 16-35 planet radius disk surrounding an undetected Jupiter-like planet is consistent with our photometry. J12 reject this model because 1/ it does not explain the F606W variability and 2/ the belt geometry would be strongly affected considering a ring-crossing orbit for Fomalhaut b (Kalas et al. 2010). As we do not find a significant F606W variability and our new astrometry cannot reject an orbit that does not cross the ring, we cannot rule out this model using the K08 arguments. J12 also consider that if the spin of the star is aligned with the plane of the disk, the north-west side of the disk is closer to Earth than the south-east side. In that case, Fomalhaut b is between its star and Earth in the radial direction and J12 claim that it would be difficult to explain how an optically thick disk can reflect so much light towards Earth. It is true if we observe the non-illuminated side of the disk but we can imagine an inclined disk such that we observe the illuminated part of the disk even if Fomalhaut b stands between Fomalhaut and Earth.

4.4. Is Fomalhaut b resolved ?

4.4.1. Extended source vs PSF

Given that a possible model for Fomalhaut b involves a cloud of dust, it would be possible that Fomalhaut b has slowly expanded in time and we test here the possibility that the Fomalhaut b HST images are slightly spatially resolved. To do so, we consider the same PSF templates as in § 4.2 and we model the object intensity distribution as a uniform disk with radius R. We convolve the object model by the PSF template and obtain the object image template T_o. We then calculate a signal-to-noise ratio SNR. The signal S is the integrated energy of the observed Fomalhaut b inside a disk of radius R+FWHM/2. The noise N is the standard deviation of the residual noise inside a 12 pixel radius disk around Fomalhaut b after subtraction of T_o. As the radius of 12 pixels is larger than R+FWHM/2, N is large if the modeled source is too large or too small to fit the data. As S and N are not calculated over the same surface, we normalize N by the square root of the ratio of the number of pixels in the 12 pixel radius disk to the number of pixels in the R+FWHM/2 radius disk. Finally, SNR is the ratio S/N.

For each radius R, we search for the flux to apply to T_o to maximize SNR. The center column in Figs. 7 and 8 give the evolution of SNR with the radius R in the 2004/F606W, 2006/F435W, 2006/F606W, 2006/F814W, and 2010/CLEAR images from top to bottom (y-scales and x-scales are not the same for all plots). The images of Fomalhaut b and of the residual noise after the best subtraction are overplotted. Note that even for the STIS data (last row), we express the radius in ACS pixels, i.e. 25 mas.

In the 2006/F814W filter (center of the fourth row), the SNR criterion is maximum for an extended source with R=5 pixels (before convolution). Fig. 9 presents the residual intensities after subtracting a PSF (center) or an extended source (right) from the Fomalhaut b image (left) at F814W. We expect to find the same size in all images but the source does not seem to be as large in the other filters (Figs. 7 and 8). This may be due to biases in our SNR criterion because of the low signal-to-noise ratio of the detections. To estimate these biases, for each filter/epoch, we add fake sources to six speckle noise dominated areas in the real images (different colors in Figs. 7 and 8) with the signal-to-noise level of Fomalhaut b and we apply the same

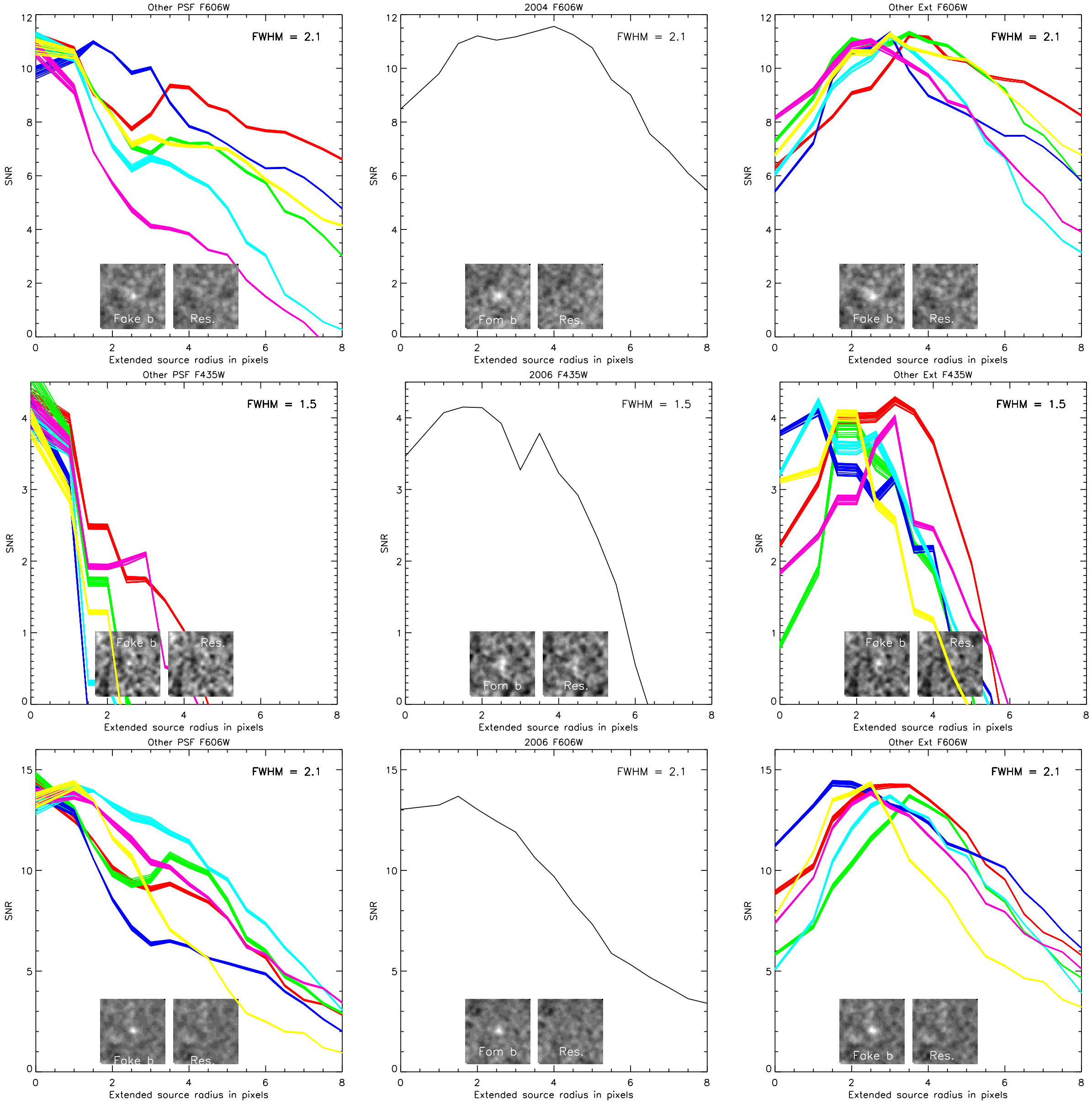

Fig. 7.— *SNR criterion as a function of the source radius in ACS pixels (25mas) for a synthetic point source (left column), the Fomalhaut b image (center column), and a synthetic extended source (right column). Top to bottom, the rows correspond to F606W in 2004, and F435W and F606W in 2006 respectively. See text for details.*

procedure to plot SNR as a function of R. We consider two different fake sources. We first assume an unresolved source (left column) and we simulate its image using 25 TinyTim PSFs at different positions on the detector (one curve per PSF). We do so to ensure that the PSF variations cannot mimic an extended source

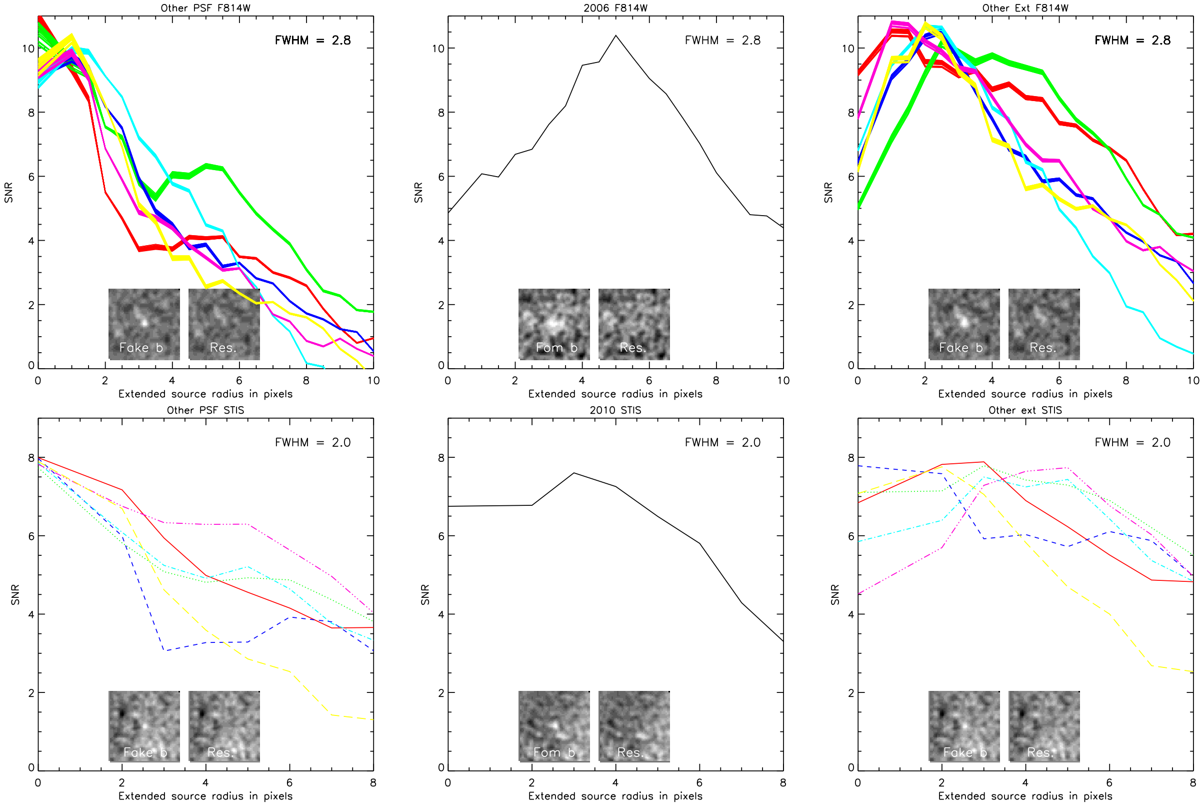

Fig. 8.— *Same as Fig. 7 for F814W in 2006 (top) and CLEAR in 2011 (bottom).*

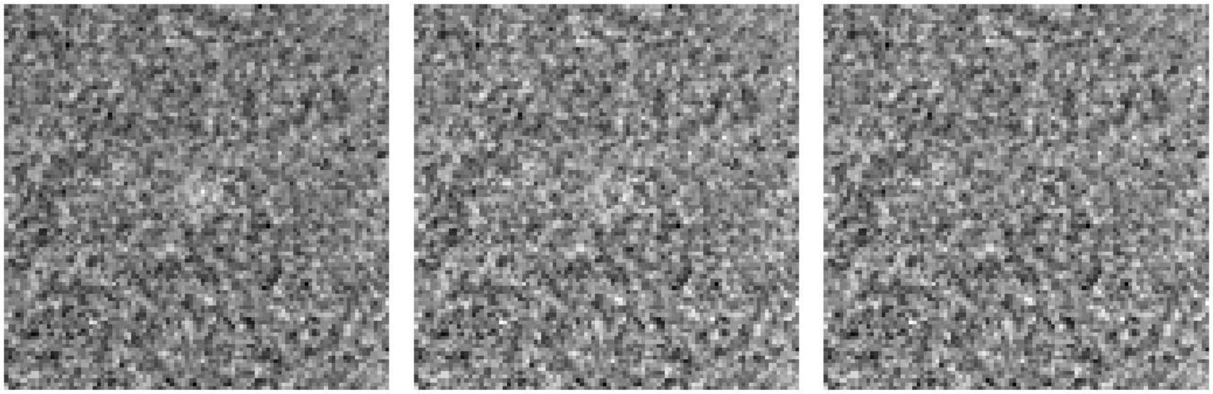

Fig. 9.— *Fomalhaut b at F814W (left) after subtracting a PSF (center) or an extended source (right).*

for our SNR criterion. The second fake source has an intensity distribution uniform in a disk with R=3 pixels before convolving with the PSF (i.e. 1.16 AU diameter, right column). We use the same 25 TinyTim PSFs to convolve the object and obtain 25 images. For the STIS data, only one fake PSF is used because the TinyTim tool does not account for the PSF variations with the positioning on the detector. For the 2006/F606W (third row), the observations (center) can be reproduced by both the point source (left) or the extended source (right). The curves of the other observations seem closer to the extended source case.

In summary, we find that the Fomalhaut b HST images are better reproduced by a slightly extended source and we choose in the rest of this section a basic model of a uniform disk with a diameter of 1.16 AU before convolution by the PSF. However, we are aware that the signal-to-noise ratios of the detections are low and that new observations are required to fully confirm this result.

4.4.2. Unlikely an instrumental effect

We investigate what instrumental effect or data processing could explain such an extended source.

The ACS/HRC PSF is contaminated by a halo for red sources, especially at F814W. The halo which adds to the "normal" PSF has a diameter (42-2.36 λ) pixels and contains a total fractional intensity $2\,(\lambda - 0.45)^3$ for the wavelength λ in microns. A 10 pixel diameter halo requires a dominant flux at $\lambda \sim 11\,\mu$m from this expression, which does not make sense because it is well outside the sensitive bandpass of the detector. Moreover, even if the signal-to-noise ratio is low, we do not observe in the F814W image a PSF plus a halo but only an extended image.

A second explanation for such an image could be a misregistering of the raw images. In that case, after the rotations that put north up in the ADI process, all the Fomalhaut b images would not fall at the exact same position, resulting in a blurred image. If this happens, any source in the field of view would be affected the same way. As the background source image (south-west) is very similar to the TinyTim PSF for the three filters (Fig. 10), we can rule out this possibility.

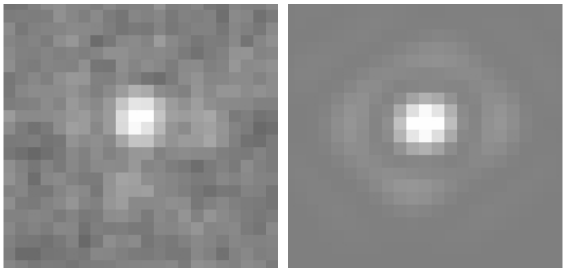

Fig. 10.— *2006 F814W image (left) and Tiny Tim model (right) of the south-west background source.*

The last instrumental effect that we foresee is a differential geometric distortion of $\gtrsim$ 1 pixel at the Fomalhaut b position between the images of a same sequence. The ACS pipeline corrects for the distortions with an accuracy 0.01 pixels (ACS handbook[2]). Thus, it would require differential distortions 100 times larger than the pipeline accuracy at the Fomalhaut b position but almost no distortions at the background source position (Fig. 10) which is roughly at the same angular separation from the star. This scenario seems very unlikely.

Finally, we find no instrumental effects that could explain the possible spatial resolution of Fomalhaut b in our images.

---

[2] http://www.stsci.edu/hst/acs/documents/handbooks/cycle20/c10_Im

4.4.3. Photometry

For each filter/epoch, we consider the template T_o for a 1.16 AU diameter object. We adjust its flux to minimize the residual noise in a 0.7" radius disk when we subtract it from the observations. For the STIS data, the disk radius for the minimization is 1.2". We follow the steps described in § 4.3.1 to convert the flux densities to Jy and estimate the error bars. The results are given in Tab. 5. As expected, the fluxes are larger than in the case of a point source. Moreover, the flux variation at F606W is larger than in the point source case but it is still less than $2.5\,\sigma_G$, thus not yet significant. An unfortunately situated speckle at less than 3 pixels from Fomalhaut b could explain this variation. Finally, the flux density measured in the large band of STIS is consistent with the average flux density measured in the ACS filters within $1.4\,\sigma_G$. In the case we resolve Fomalhaut b, we plot the photometry of our detections (crosses) in Fig. 11.

Date	Filter	Flux density (μJy)
2004	F606W	1.09±0.13
2006	F435W	0.71±0.14
2006	F606W	0.67±0.11
2006	F814W	0.62±0.12
2010	CLEAR	1.26±0.34

Table 5: *Photometry if Fomalhaut b is 1.16 AU large.*

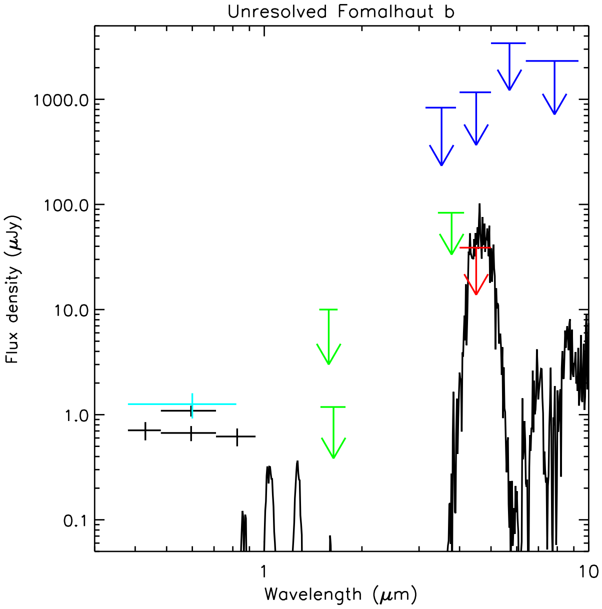

Fig. 11.— *Same as Fig. 6 in the case the object is resolved.*

The models presented in sections 4.3.2 and 4.3.3 of a planet surrounded by a dust disk and a cloud of dust are both introduced in K08 in the case Fomalhaut b is not resolved. In the case of a spatially resolved Fomalhaut b, we propose one basic model that assume that Fomalhaut b is the result of the collision of two Kuiper belt objects (§ 4.4.4) and we adapt a model of circumplanetary swarm of satellites (§ 4.4.5) proposed by Kennedy&Wyatt (2011).

4.4.4. Collision of Kuiper belt objects

In this section, we propose a basic model to roughly estimate the size and the amount of light that is scattered by a cloud of dust produced by the collision of two Kuiper belt objects (KBO). The objective is not to derive the exact radius, mass and velocity of the KBOs that could create Fomalhaut b but to show that the collision of two KBOs is not completely inconsistent with the observations. First, we estimate the total grain mass that can explain the fluxes received from Fomalhaut b. Then, we show that the amount of dust can be the result of a collision of two 50 km radius colliders. We evaluate the rate of collisions of two such KBOs around Fomalhaut. Finally, we estimate when the collision may have occurred to reproduce the size of the Fomalhaut b images.

If the particles of dust are spheres with radius a and if the cross section of the particles equals their geometric albedo, the mass M_d of a cloud of dust that lies at a distance D from its star is (Jura et al. 1995)

$$M_d \gtrsim \frac{16\,\pi}{3}\,\rho\,D^2\,a\,\frac{L_{sc}}{L_*} \qquad (4)$$

where ρ is the mass density of the dust grains, and L_{sc} and L_* are the luminosity of the light scattered by the cloud and the luminosity of the star respectively. Instead of estimating the ratio of the luminosities, we work with the fluxes F_{sc} and F_* received at the telescope. We estimate F_{sc} from the measured fluxes (F_i) in the ACS filters (i=F435W, F606W, and F814W, Tab. 5)

$$F_{sc} = \sum_i F_i \Delta\nu_i \qquad (5)$$

with $\Delta\nu_i$ the bandwidths of the filters. Our estimation of F_{sc} only includes the scattered energy in the F435W, F606W and F814W bandpasses. F_* has to be calculated for the same bandpass. Assuming a Planck law, F_* in the bandpass $[\lambda_{min} = 435 - 50\,\mathrm{nm}, \lambda_{max} = 825 + 115\,\mathrm{nm}]$ is

$$F_* = F_{*,tot}\,\frac{\int_{u_{min}}^{u_{max}} u^3/(\exp u - 1)\,\mathrm{d}u}{\int_0^\infty u^3/(\exp u - 1)\,\mathrm{d}u} \qquad (6)$$

where $u_{min,max} = h\,c/(k\,T\,\lambda_{max,min})$ with the Planck constant h, the speed of light in vacuum c, the Boltzmann constant k, the stellar effective temperature T (8751 K, Di Folco et al. 2004), and the stellar flux $F_{*,tot}$ received at the telescope (8.914e-6 erg.cm^{-2}, Kalas et al. 2008). For $D \sim 120$ AU and dust grains with radius a =10 μm and $\rho = 2$ g.cm^{-3}, we find from Eqs. 4, 5, and 6 that the total grain mass needed to reproduce the photometry of Fomalhaut b is $M_\mathrm{d} \sim 4.10^{19}$ g.

Jewitt (2012) estimates the mass m_e of particles that are ejected after a collision of two KBOs with a mass M_kbo, a radius r, a density ρ, and a relative velocity U

$$\frac{m_\mathrm{e}}{M_\mathrm{kbo}} = A\left[r\,\sqrt{\frac{8\,\pi\,G\,\rho}{3}}\right]^{-1.5} U^{1.5} \qquad (7)$$

where A equals 0.01 and $G = 6.67\,10^{-11}$ m^3 kg^{-1} s^{-2} is the gravitational constant. Jewitt (2012) assumes the particles have radii in the range $0.1\,\mu\mathrm{m} \lesssim a \lesssim 0.1$ m with a power law distribution in radii with index ~ 3.5 (see also Kadono et al. 2010). For typical KBOs in the ring, U is the orbital velocity times $h_r/(2D)$ with h_r the full vertical height of the ring at radius D. With $h_r \sim 3.5$ AU (Kalas et al. 2005) at $D \sim 120$ AU, U is close to 60 m s^{-1}. Assuming KBOs with radius $r = 50$ km, the total debris mass m_e after the collision is roughly 1% of the mass M_kbo of one of the two colliders with a density $\rho = 2$ g cm^{-3}. Given the approximations in the models, the expected mass of dust (1% M_kbo) that is ejected after a collision of two 50 km radius KBOs is consistent with the mass estimated from the photometry of Fomalhaut b (4 % M_kbo for a 50 km radius KBO).

If the escape velocity $r\,\sqrt{8\,\pi\,G\,\rho/3}$ is the average velocity of the particles, the diameter s of the cloud is $2\,r\,t\,\sqrt{8\,\pi\,G\,\rho/3}$ at the date t after the collision. To reproduce the observed size $s = 1.16\,\mathrm{AU}$ (§ 4.4.1), the collision should have occurred ~ 50 years ago. We can also estimate from this expression that after ~ 200 years, the source would have a diameter $\sim 4\,\mathrm{AU}$ and would be ~ 10 times fainter than the current detections assuming the same amount of reflecting dust. It would not be detected in our images. As the size of the possible extended source is very approximative, we keep in mind that these numbers are coarse estimations.

Finally, we evaluate the rate of a collision of two $r = 50\,\mathrm{km}$ KBOs at the Fomalhaut b position. We first find the collision time which reads

$$t_{\rm col} = \frac{1}{4\,\pi\,n\,r^2}\,\frac{1}{U} \tag{8}$$

with n the number of KBOs with radius r per unit volume. To estimate n we need the mass $M_{\rm disk}$ of the debris disk around Fomalhaut. We assume $M_{\rm disk}$=40 $M_{\rm Earth}$ because 1/ estimates of the mass of the Sun's early Kuiper belt is 40 $M_{\rm Earth}$ (Schlichting&Sari 2006), and 2/ estimates of the mass of the Vega debris belt is 10 $M_{\rm Earth}$ in objects with radii $< 100\,\mathrm{km}$ (Müller et al. 2010) whereas the Vega IR luminosity is 4 times fainter than that of Fomalhaut. Simplifying by setting the radii of all the KBOs to 50 km does not qualitatively alter the collision frequency estimated below. Under these conditions and considering the belt surrounding Fomalhaut A has a volume $2\,\pi\,D\,\Delta D\,h_r$ with $\Delta D \sim 0.13\,D$ (Kalas et al. 2005), the number of KBOs is

$$n\,2\,\pi\,D\,\Delta D\,h_r = \frac{M_{\rm disk}}{M_{\rm kbo}} \sim 2\times 10^8 \tag{9}$$

Using $U = \pi\,h\sqrt{M_*/M_\odot\,(1\mathrm{AU}/D)^3}$, and Eqs. 8 and 9, we can write

$$t_{\rm col} = \frac{0.13}{2\,\pi}\left(\frac{D}{r}\right)^2\frac{M_{\rm kbo}}{M_{\rm disk}}\sqrt{\left(\frac{D}{1\mathrm{AU}}\right)^3\frac{M_\odot}{M_*}} \tag{10}$$

Finally, the rate κ of collisions of two KBOs with radii r is the ratio of the number of KBOs (Eq. 9) to $t_{\rm col}$

$$\kappa = \frac{2\,\pi}{0.13}\left(\frac{r}{D}\right)^2\left(\frac{M_{\rm disk}}{M_{\rm kbo}}\right)^2\sqrt{\left(\frac{1\mathrm{AU}}{D}\right)^3\frac{M_*}{M_\odot}} \tag{11}$$

Eq. 11 with $M_{\rm disk} = 40\,M_{\rm Earth}$, and $M_* = 2\,M_\odot$ indicates that ~ 1 collision of two $r = 50\,\mathrm{km}$ KBOs occurs every century in the ring around Fomalhaut A. Even if the rate at the Fomalhaut b position may be lower, given the approximations of our model the rate is high enough to make such a ~ 50 year-old event plausible. At the same time, it is low enough to explain that we detect only one event around Fomalhaut as each event would be detectable during ~ 200 years in our images.

In summary, we conclude that it is plausible that Fomalhaut b is a cloud of dust that was produced ~ 50 years ago by the collision of two KBOs with radii $\sim 50\,\mathrm{km}$.

4.4.5. Circumplanetary satellite swarm

Kennedy&Wyatt (2011, K11) propose a model of circumplanetary satellite swarms that they apply to Fomalhaut b. They find that the planet mass can be $\sim$2-100 $M_{\rm Earth}$ surrounded by a swarm that lies at 0.1-0.4 Hill radii. The swarm mass would be of the order of a few lunar masses. But these numbers are derived from K08 photometry of an unresolved source.

Here, we use the same model under the same assumptions (body size distribution and maximum/minimum body sizes, dust density, etc) but we consider a swarm of satellites with diameter 1.16 AU, our photometry (Tab. 5), and a star with age 440 Myr instead of 200 Myr (Mamajek 2012). We do not describe the model as it is done in K11. We only use the meaningful equations to constrain the planet mass and the swarm mass and size following the steps in § 3.3.1 and § 3.3.2 of K11. First, we derive the total cross-sectional area of dust $\sigma_{\rm tot}$ from our photometry: $\sigma_{\rm tot} = 7.22 \times 10^{-4} {\rm au}^2$, assuming a geometric albedo 0.08, a phase function 0.32 (Lambert sphere at maximum extension from its host star), the star effective temperature 8,751 K (Di Folco et al. 2004), and a stellar luminosity 6.34.10^{27} W (K08).

As we assume that we resolve Fomalhaut b, we can write $2\,\eta\,R_{\rm Hill} = s$, where η is the semimajor axis of the satellites of the swarm relative to the Hill radius $R_{\rm Hill}$ at the Fomalhaut b separation (118 AU) and s is the swarm diameter. As $s =$ 1.16 AU is an approximative size (§ 4.4.1), we consider 1.16 AU< s <2.32 AU. Using the Hill radius expression and 2 solar masses for Fomalhaut (K11), we derive two constraints: $0.62/M_{\rm pl}^{1/3} < \eta < 1.24/M_{\rm pl}^{1/3}$, where $M_{\rm pl}$ is the planet mass.

If the cloud is optically thick and the dust is uniformly projected on the sky across $\pi\,(\eta\,R_{\rm Hill})^2$, the geometrical optical depth $\tau = \sigma_{\rm tot}/(\pi(\eta\,R_{\rm Hill})^2)$ is smaller than 1 (K11), which sets $\eta > 0.017/M_{\rm pl}^{1/3}$.

Then, considering a collision-limited satellite swarm around Fomalhaut b (i.e. swarm has just started to suffer collisions) that reproduces the observed $\sigma_{\rm tot}$, it imposes a minimum limit for the satellite semimajor axis $\eta > 0.33/M_{\rm pl}^{0.12}$ for a 440 Myr system (see K11 for details).

K11 also study the collision velocities that are required to destroy a large object at the Fomalhaut b position. Using their expressions in the case of a resolved object we set a constraint that reads $\eta > 0.71/M_{\rm pl}^{0.46}$ (K11).

Moreover, K11 assumed that satellite orbits with $\eta > 0.5$ are not stable and did not consider them. Finally, we account for the 1 M$_J$ upper limit that Janson et al. (2012) put from the non detection at 4.5μm for a 400 Myr system (close enough to 440 ± 40 Myr proposed by Mamajek 2012). We plot all the constraints in Fig. 12 that gives the semimajor axis η of the satellites against the planetary mass $M_{\rm pl}$. The parameters for

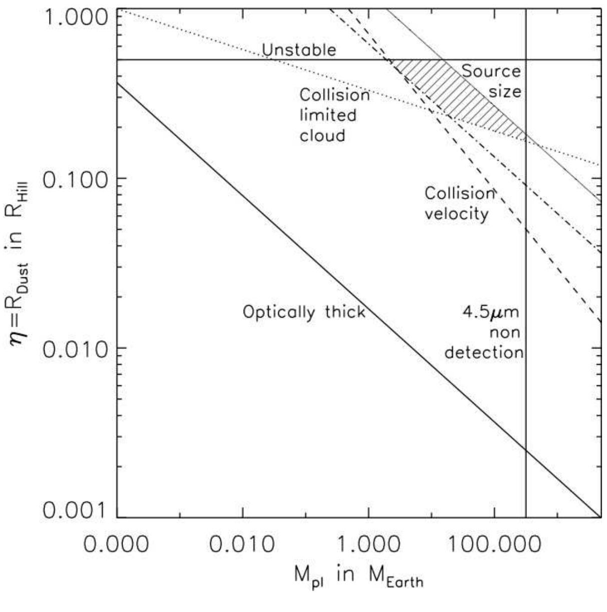

Fig. 12.— *Semimajor axis η of satellites of the swarm versus planetary mass $M_{\rm pl}$ diagram that shows the different constraints derived in the text. The parameters that could explain the Fomalhaut b images are inside the dashed region.*

which K11's model can reproduce the photometry of a 1.16 AU source are within the dashed area. The minimum and maximum planetary masses are $\sim 2\,M_{\rm Earth}$ and $1\,M_J$ and the swarm has a total mass 3-12 $M_{\rm Moon}$ and lies at 0.17-0.5 Hill radii around the planet.

In the case of an unresolved object (Fig. 7 in K11), K11 find that the mass of the planet ($< 100\,M_{\rm Earth}$) is not sufficient for it to have a significant gaseous envelope and enable mechanisms that could explain the migration of Fomalhaut b that presumably originates somewhere closer to the star. K11 also argue that a single planet with mass $< 100\,M_{\rm Earth}$ – which is similar or less than the mass of the main debris ring (1-300 $M_{\rm Earth}$, Wyatt&Dent 2002; Chiang et al. 2009) – is unlikely responsible for shaping the dust belt. In our case of a source with diameter 1.16 AU, the range of the planetary mass goes up to $1\,M_J$ and a Jupiter-like planet can have a significant gaseous envelope and shape the dust belt.

5. Conclusions

Our independent analysis of the ACS and STIS data taken in 2004, 2006, and 2010 confirms that Fomalhaut b is real and is not a speckle artifact as we clearly detect the object at the three epochs at several filters (Figs. 1, 2, and 3). In this way, we confirm the Kalas et al. (2008, K08) detection. However, we find differences in our analysis concerning astrometry and photometry of Fomalhaut b.

Unlike Kalas et al. (2010), we cannot affirm that the object follows a trajectory that crosses the belt of dust because our astrometry is consistent within $1.1\,\sigma$ with crossing and non-crossing orbits (§ 4.2).

We detect Fomalhaut b in the short wavelength filter F435W whereas K08 find an upper limit. In the case of an unresolved source, our photometry is consistent with K08 at F606W/2004 and F814W/2006 but differs at F606W in the 2006 data (§ 4.3.1). As a consequence, unlike K08, we detect no significant variability of the F606W flux between 2004 and 2006. Considering the reduced and possible lack of variability at F606W and the detection at F435W, several dust cloud models discussed by K08 cannot be ruled out anymore (§ 4.3.2). K08 propose also a model of a Jovian planet surrounded by a large disk of dust. Janson et al. (2012) exclude this explanation mainly because of the variability at F606W and the assumed dust belt crossing trajectory. Given our new photometry and astrometry, we cannot reject this model (§ 4.3.3).

In the second part of our analysis, we study the possibility that Fomalhaut b is spatially resolved in our images. The signal-to-noise ratios of the detections are low and more data are required to confirm the result but we find that our images are more consistent with an extended source with diameter 1.16 AU than with a point source (§ 4.4.1 and 4.4.2). The photometric variability of an extended source model at F606W is larger than for a point source but it is not yet significant ($< 2.5\,\sigma$, § 4.4.3). Two models are considered to explain the size and the photometry of an extended source. First, the measurements are consistent with a cloud of dust produced by a collision of two Kuiper belt objects with radius 50 km that would have occurred $\sim$ 50 years ago (§ 4.4.4). The second model is an adaptation of the circumplanetary satellite swarm model proposed by Kennedy&Wyatt (2011). It is consistent with the data when considering a $2\,M_{\mathrm{Earth}}$-$1\,M_J$ planet surrounded by a swarm that lies at 0.17-0.5 Hill radii (§ 4.4.5).

The nature of the Fomalhaut b object is still uncertain. However, from the two independent analysis of the HST data by K08 and our team, we can claim that Fomalhaut b is a real object that orbits Fomalhaut A.

6. Acknowledgment

The authors are grateful to the ACS team, John Blakeslee, and Travis Barman for helpful discussions. The authors also thank Paul Kalas and James Graham for useful communications on their analysis. Partial financial support for this research came from a NASA grant to UCLA.

REFERENCES

Acke, B., et. al., 2012, *The Astrophysical Journal*, **540**, A125.

Boley, B., et. al., 2012, *The Astrophysical Journal Letters*, **750**, L21.

Chiang, E., and Kite, E., and Kalas, P., and Graham, J. R., and Clampin, M., 2009, *The Astrophysical Journal*, **693**, 734–749.

Di Folco, E., et al., 2004, *Astronomy and Astrophysics*, **426**, 601-617.

Janson, M., et al., 2012, *The Astrophysical Journal*, **747**, id. 116 (J12).

Jewitt, D., 2012, *The Astronomical Journal*, **143**, id. 66.

Jura, M., et al., 1995, *The Astrophysical Journal, Part 1*, **445**, 451–456.

Kadono, T., et al., 2010, *Earth, Planets, and Space*, **62**, 13–16.

Kalas, P., Graham, J. R., Clampin, M., 2005, *Nature*, **435**, 1067–1070.

Kalas, P., et al., 2008, *Science*, **322**, 1345– (K08).

Kalas, P., Graham, J., Fitzgerald, M., and Clampin, M., 2010, *In the Spirit of Lyot 2010*, Update on Fomalhaut b.

Kennedy, G. M., and Wyatt, M. C., 2011, *Monthly Notices of the Royal Astronomical Society*, **412**, 2137–2153 (K11).

Krist, J., Hook, R., Stoehr, F., 2011, *SPIE*, **8127**.

Lafrenière, D., Marois, C., Doyon, R., Nadeau, D., Artigau, É, 2007, *The Astrophysical Journal*, **660**, 770–780.

Lagrange, A. M., et al., 2009, *Astronomy and Astrophysics*, **493**, L21-L25.

Mamajek, E. E., 2012, *The Astrophysical Journal Letter*, **754**, L20.

Marengo, M., et al., 2009, *The Astrophysical Journal*, **700**, 1647–1657.

Marois, C., Lafrenière, D., Doyon, R., Macintosh, B., Nadeau, D., 2006, *The Astrophysical Journal*, **641**, 556–564.

Marois, C., et al., 2008, *Science*, **322**, 1348–.

Marois, C., Zuckerman, B., Konopacky, Q. M., Macintosh, B., Barman, T., 2010, *Nature*, **468**, 1080–1083.

Marois, C., Macintosh, B., Véran, J.-P., 2010b, *SPIE*, **7736**.

Mouillet, D., Larwood, J. D., Papaloizou, J. C. B, Lagrange, A. M., 2010b, *Monthly Notices of the Royal Astronomical Society*, **292**, 896–.

Müller, S., Löhne, T. and Krivov, A. V., 2010, *The Astrophysical Journal*, **728**, 1728–1747.

Quillen, A. C., 2006, *Monthly Notices of the Royal Astronomical Society*, **372**, L14–L18.

Schlichting, H. E., and Sari, R., 2011, *The Astrophysical Journal*, **728**, id.68.

Spiegel, D. S., and Burrows, A., R., 2012, *The Astrophysical Journal*, **745**, 174.

Van Leeuwen, F., 2012, *Astronomy and Astrophysics*, **474**, 653–664.

Wyatt, M. C., et al., 1999, *The Astrophysical Journal*, **527**, 918–944.

Wyatt, M. C., and Dent, W. R. F., 2002, *Monthly Notices of the Royal Astronomical Society*, **334**, 589–607.

This 2-column preprint was prepared with the AAS LaTeX macros v5.2.